Letters

A Noncommunication Mutual Inductance Estimation Method for Multiple Transmitters SS-Compensated Dynamic Wireless Power Transfer With Low Calculation Effort

Kaiwen Chen, *Member, IEEE*, Zhenghua Nie, Chongxu Yan, Norbert Chow Cheung, *Senior Member, IEEE*, Eric Ka-Wai Cheng, *Fellow, IEEE*, and Jianfei Pan, *Member, IEEE*

***Abstract*—Mutual inductance estimation (MIE) plays an essential role in the primary-side control for dynamic wireless power transfer (DWPT) systems. Traditional MIE method that is only based on primary-side transmitter (*Tx*) information contributes to no redundant hardware components. However, this method can cause huge calculation effort in multi-*Tx*s DWPT systems because it involves the solution of multivariable multiple equations. In this letter, a new method for estimating mutual inductance for series–series (SS)-compensated multi-*Tx*s DWPT systems is proposed, where dual-side communication and auxiliary position sensor are not required. By first solving the mutual inductance ratio and then calculating the exact mutual inductance, the proposed method is proven to avoid solving multiple equations, thus greatly reducing complexity of the calculation. This study also includes simulations and experiments that are carried out in a DWPT system with two *Tx*s to one receiver (*Rx*).**

***Index Terms*—Dynamic wireless power transfer (DWPT), mutual inductance estimation (MIE), noncommunication.**

I. Introduction

THE wireless power transfer (WPT) technology, as an ideal alternative to cabled charging, has raised much attention of world-wide researchers and commercialized entities, due to its safety and convenience [1]. In recent years, dynamic wireless power transfer (DWPT) had made much contribution to the charging scheme for moving electric applications [2]. For achieving the desired output and with high efficiency, numerous primary-side control methods for the DWPT system were proposed [3], [4]. The mutual inductance estimation (MIE) method is the key link that is always needed in these control methods.

Monitoring of electrical information is indispensable during the MIE implementation. The monitoring methods can be divided into two categories: 1) integration of dual-side communication to collect both sides information, and 2) monitoring only the primary-side information. In the first method, the current and voltage of the secondary side can be transmitted back by a dual-side communication module (e.g., Wi-Fi and Bluetooth), and then, the mutual inductance can be calculated directly by combining the information from the primary side [5], [6], [7]. Nevertheless, in dynamic conditions, the delay caused by the communication link and the handshake process can deteriorate the dynamic performance of the control and reduce the reliability of the system. As to the second method, the system is mathematically modeled by applying Kirchhoff's voltage law (KVL), and then, the mutual inductance can be estimated by collecting the primary-side information and solving the multiple equations with one variable [8], [9], [10]. Although it has been proven to be effective in the topology with a single transmitter (i.e., *Tx*), it needs to solve multivariable high-order equations under the case of the multiple *Tx*s (i.e., multi-*Tx*s) DWPT, which will involve huge calculation effort and cumulative error. It is necessary to reduce the calculation effort because the control loop can have better dynamic performance when the *Rx* is with faster movement [11], [12]. Hence, a noncommunication MIE method for calculation reduction should be investigated for the multi-*Tx*s DWPT systems.

This letter proposed a new MIE method for series–series (SS)-compensated multi-*Tx*s DWPT systems. The proposed method first calculates the mutual inductance ratio, and then estimates the exact value of mutual inductance. Only the primary-side information is required, and the dual-side communication and auxiliary coils are not introduced. The contributions of this letter can be summarized as follows.

1) *Low calculation effort:* The complicated solution of multivariable multiple equations in the traditional primary-side MIE is not involved.

Manuscript received 23 January 2024; revised 25 February 2024; accepted 16 March 2024. Date of publication 25 March 2024; date of current version 16 May 2024. This work was supported in part by the Research Grants Council General Research Fund Grant Hong Kong under Grant 15225422, in part by the National Natural Science Foundation of China under Grant 52277060, and in part by the Shenzhen Science and Technology Program under Grant JCYJ20220818100000001 and Grant SGDX20230116110009018. *(Corresponding author: Eric Ka-Wai Cheng.)*

Kaiwen Chen and Eric Ka-Wai Cheng are with the Power Electronics Research Centre, Department of Electrical and Electronic Engineering, Hongkong Polytechnic University, Kowloon 999077, Hong Kong (e-mail: eric-cheng.cheng@polyu.edu.hk).

Zhenghua Nie, Chongxu Yan, Norbert Chow Cheung, and Jianfei Pan are with the Guangdong Key Laboratory of Electromagnetic Control and Intelligent Robots, College of Mechatronics and Control Engineering, Shenzhen University, Shenzhen 518060, China.

Color versions of one or more figures in this article are available at https://doi.org/10.1109/TPEL.2024.3379951.

Digital Object Identifier 10.1109/TPEL.2024.3379951

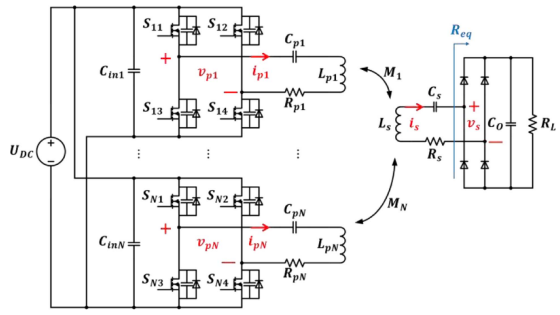

Fig. 1. Circuitry diagram of SS-compensated multi-*Tx*s DWPT system.

2) *Feasible in multi-Txs DWPT system:* The proposed MIE method is derived based on *N Tx*s DWPT system, and no additional power switch is utilized.
3) *Low cost and high reliability:* The communication unit and redundant circuit component are not required.

II. Modeling of the Multi-Txs DWPT System and Derivation of the Proposed MIE Method

A. Mathematical Modeling of the System

The circuit of the SS-compensated DWPT system with *N Tx*s is illustrated in Fig. 1. In the following sections, i stands for the *i*th *Tx*. The direct current (dc) voltage (i.e., $U_{\rm dc}$) is converted into alternative current (ac) squared-wave voltages (i.e., v_{pi}) as the input voltage for primary windings by the primary inverter, which consists of four MOSFET, (i.e., S_{i1}–S_{i4}). The inductances (i.e., L_{pi} and L_s) are compensated with series-connected capacitors (i.e., C_{pi} and C_s). The resistances (i.e., R_{pi} and R_s) stand for the sum of the copper resistance and the equivalent series resistance (ESR) of the capacitor. M_i stand for the mutual inductance between the *i*th *Tx* and *Rx*. The ac magnetic field generated by L_{pi} is collected by the *Rx* coupler, and then it is transformed to ac secondary voltage (i.e., v_s). v_s is rectified into dc power by the full-bridge rectifier for powering the load (i.e., R_L). $R_{\rm eq}$ is the equivalent resistance that is seen before the rectifier.

Since the *Tx*s are similarly designed and compensated, they share the same electrical parameters, which means that $R_{p1} = R_{p2} = \cdots = R_{pN} = R_p$, $L_{p1} = L_{p2} = \cdots = L_{pN} = L_p$, and $C_{p1} = C_{p2} = \cdots = C_{pN} = C_p$. In order to mathematically model the multi-*Tx*s DWPT system, KVL is adopted to analyze the primary and secondary circuits in complex frequency domain. Hence, the following can be obtained:

$$\begin{bmatrix} v_{p1} \\ v_{p2} \\ \vdots \\ v_{pN} \\ 0 \end{bmatrix} = \begin{bmatrix} R_p + jX_p & 0 & \dots & 0 & j\omega M_1 \\ 0 & R_p + jX_p & \dots & 0 & j\omega M_2 \\ \vdots & \vdots & \ddots & \vdots & \vdots \\ 0 & 0 & 0 & R_p + jX_p & j\omega M_N \\ j\omega M_1 & j\omega M_2 & 0 & \dots & R_{eq} + R_s + jX_s \end{bmatrix} \times \begin{bmatrix} i_{p1} \\ i_{p2} \\ \vdots \\ i_{pN} \\ i_s \end{bmatrix} \tag{1}$$

where ω is the angular operation frequency. The dc components, such as $U_{\rm dc}$ and $R_{\rm eq}$, can be linked with their ac components by adopting the Fourier transform and extracting fundamental-wave components, which are as follows:

$$\begin{cases} R_{\rm eq} = \frac{8}{\pi^2} R_L \\ v_{pi} = \frac{4}{\pi} U_{dc},\ i = 1,\ 2, \dots, N. \end{cases} \tag{2}$$

In (1), M_i is the mutual inductance between ith *Tx* and *Rx*, and X_p and X_s stand for the primary and secondary winding impedance. Because the L_p and L_s are fully compensated, the winding impedance is about negligible in the operation frequency (i.e., ω)

$$\begin{cases} X_p = j\omega L_p + 1/j\omega C_p = 0 \\ X_s = j\omega L_s + 1/j\omega C_s = 0. \end{cases} \tag{3}$$

The primary winding current (i.e., i_{pi}) can be deduced from (1) as follows:

$$i_{pi} = \frac{\left(R_p R_{\rm eq} + \omega^2 \sum_{k=1,\ k\neq i}^{N} M_k^2\right) v_{pi} - \omega^2 M_i \sum_{k=1,\ k\neq i}^{N} M_k v_{pk}}{\tau} \tag{4}$$

where $i = 1,\ 2, .., N$, and τ is always larger than 0, which can be expressed as follows:

$$\tau = R_p \left(\omega^2 \sum_{k=1}^{N} M_k^2 + R_p R_{\rm eq}\right). \tag{5}$$

It is assumed that the mutual inductance ratio between ith *Tx* with *Rx* and jth *Tx* with *Rx* is γ_{ij}, which is defined as

$$\gamma_{ij} = \frac{M_i}{M_j}. \tag{6}$$

If the numerator and denominator of (4) is divided by M_g^2, (4) can be rewritten as

$$i_{pi} = \frac{\left[\frac{R_p R_{\rm eq}}{M_g^2} + \omega^2 \sum_{k=1,\ k\neq i}^{N} \gamma_{kg}^2\right] v_{pi} - \omega^2 \gamma_{ij} \sum_{k=1,\ k\neq i}^{N} \gamma_{kg} v_{pk}}{\tau_g} \tag{7}$$

where τ_g is still larger than 0, which is

$$\tau_g = R_p \left[\omega^2 \sum_{k=1}^{N} \gamma_{kg}^2 + \frac{R_p R_{\rm eq}}{M_g^2}\right]. \tag{8}$$

According to the definition in (6), there are two properties that can be easily derived as

$$\begin{cases} \gamma_{ii} = M_i/M_i = 1 \\ \gamma_{ij} = 1/\gamma_{ji}. \end{cases} \tag{9}$$

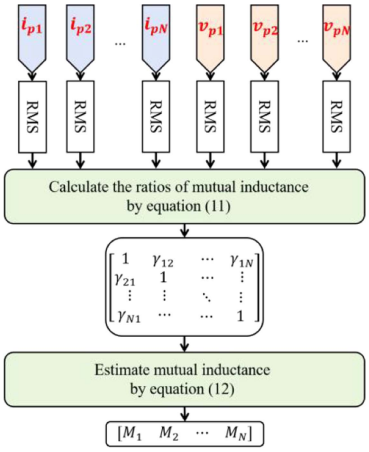

Fig. 2. Implementation flowchart diagram of the proposed MIE method.

B. Derivation of the Proposed MIE Method

By expanding (5), the component $R_p R_{\text{eq}}/M_j^2$ can be equal to multiple equations, which are

$$\begin{cases} \frac{R_p R_{\text{eq}}}{M_g^2} = \omega^2 \frac{\gamma_{1g}\left(\sum_{k=2}^{N} \gamma_{kg} v_{pk} + \gamma_{1g} i_{p1} R_p\right)}{v_{p1} - i_{p1} R_p} - \omega^2 \sum_{k=2}^{N} \gamma_{kg}^2 \\ \frac{R_p R_{\text{eq}}}{M_g^2} = \omega^2 \frac{\gamma_{2g}\left(\sum_{k=1,\ k\neq 2}^{N} \gamma_{kg} v_{pk} + \gamma_{2g} i_{p2} R_p\right)}{v_{p2} - i_{p2} R_p} \\ \quad -\omega^2 \sum_{k=1,\ k\neq 2}^{N} \gamma_{kg}^2 \\ \qquad \vdots \\ \frac{R_p R_{\text{eq}}}{M_g^2} = \omega^2 \frac{\gamma_{Ng}\left(\sum_{k=1}^{N-1} \gamma_{kg} v_{pk} + \gamma_{Ng} i_{p1} R_p\right)}{v_{pN} - i_{pN} R_p} - \omega^2 \sum_{k=1}^{N-1} \gamma_{kg}^2. \end{cases} \tag{10}$$

Through applying elimination method in (9) by multiple times, the mutual inductance ratio can be derived as follows:

$$\gamma_{ig} = \frac{v_{pi} - i_{pi} R_p}{v_{pg} - i_{pg} R_p}. \tag{11}$$

By substituting (10) into (6), the exact value of gth Tx can be calculated by

$$M_g = \frac{1}{\omega} \sqrt{\frac{R_{eq}\left(v_{pg} - i_{pg} R_p\right)}{\sum_{k=1}^{N} \gamma_{kg} i_{pk}}} = \frac{1}{\omega} \sqrt{\frac{R_{eq}\left(v_{pg} - i_{pg} R_p\right)}{\sum_{k=1}^{N} i_{pk} \frac{v_{pk} - i_{pk} R_p}{v_{pg} - i_{pg} R_p}}}. \tag{12}$$

III. Implementation of the Proposed MIE Method

Fig. 2 shows the implementation flowchart of the proposed MIE method. The currents of *Txs* and the input winding ac voltages are sampled in real time. The root-mean-square (rms) values of the monitored currents and voltages are calculated, and then the mutual inductance ratio matrix is calculated by (11). Finally, based on the mutual inductance ratio matrix, the mutual inductance between every *Tx* coil and the *Rx* coil can be estimated by (12).

It is worth mentioning that the operation frequency (i.e., ω), equivalent load resistance (i.e., R_{eq}) and the primary winding ESR (i.e., R_p) are determined as preconditions before the operation of the proposed MIE method. In order to guarantee the load to be pure resistance, the power factor correction should be integrated in practice of the proposed method, which can be commonly seen in the DWPT system [13], [14], [15].

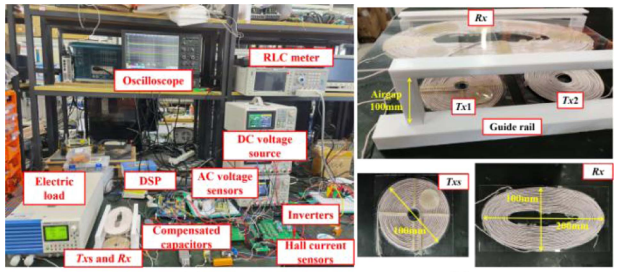

(a) (b)

Fig. 3. Experimental platform. (a) Key components and measurement equipment. (b) Couplers and moving mechanism.

TABLE I
Parameters of the Main Components and Conditions in Experiments and Simulations (Temperature: 25 °C)

Parameter	Value	Parameter	Value
L_{p1}	30.45 μH	C_{p1}	115.25 nF
L_{p2}	31.25 μH	C_{p2}	115.25 nF
L_s	64.4 μH	C_s	54.5 nF
C_{in}	1000 μF	C_f	200 μF
R_{p1}	5.13 Ω	R_{p2}	5.15 Ω
R_s	2.02 Ω	R_{eq}	50 Ω
M_1	0.86 –19.78 μH	M_2	19.53 – 23.76 μH
f	85 kHz	U_{dc}	24 V

IV. Simulation and Experimental Verification

A. Experimental Setup

In order to verify the proposed MIE method, a prototype of a DWPT system with two *Tx*s (i.e., *Tx*1 and *Tx*2) and one *Rx* is constructed. The experimental platform and key measurement equipment are demonstrated in Fig. 3. The DWPT system consists of a programmable dc voltage source, two full-bridge inverters, a digital signal processor (DSP), inductive couplers, a full-bridge rectifier, and an electronic load. An oscilloscope, two current probes, and two ac voltage probes are used for collecting key waveforms in experiments, and the ac voltage sensors and hall current sensors are used for sampling the primary electrical information for DSP process. The coupler that includes two *Txs* to one *Rx* is shown in Fig. 3(b). Both the *Tx* coil and the *Rx* coil are stranded in circular shape, and their sizes are 100 mm $\times$100 mm and 100 mm $\times$ 200 mm, respectively. The couplers are with air cores, and the air gap between *Txs* and *Rx* is 100 mm. The couplers can be moved laterally on the guide track to create varying coupling conditions.

The key parameters in the experiments and simulations are listed in Table I. The resonant and operation frequency are the same at 85 kHz. The MOSFET used in the experiment is Infineon F4-23MR12W1M1-B11 full-bridge MOSFET module,

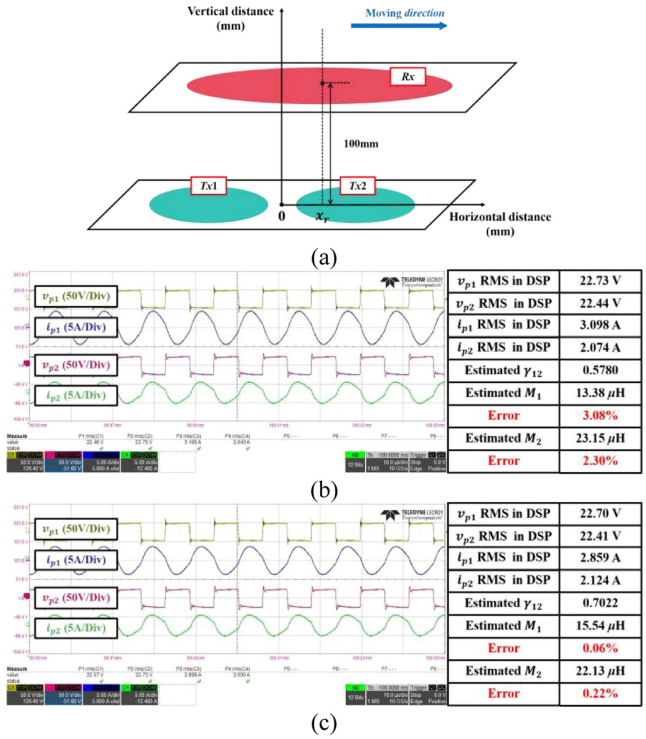

v_{p1} RMS in DSP	22.73 V
v_{p2} RMS in DSP	22.44 V
i_{p1} RMS in DSP	3.098 A
i_{p2} RMS in DSP	2.074 A
Estimated γ_{12}	0.5780
Estimated M_1	13.38 μH
Error	3.08%
Estimated M_2	23.15 μH
Error	2.30%

v_{p1} RMS in DSP	22.70 V
v_{p2} RMS in DSP	22.41 V
i_{p1} RMS in DSP	2.859 A
i_{p2} RMS in DSP	2.124 A
Estimated γ_{12}	0.7022
Estimated M_1	15.54 μH
Error	0.06%
Estimated M_2	22.13 μH
Error	0.22%

Fig. 4. Experiment and simulation verifications of the proposed MIE method. (a) Horizontal movement of the *Rx*. (b) Case 1 (x_r =15 mm, $M_1 = 12.98$ μH, M_2 =22.63 μH). (c) Case 2 (x_r =10 mm, M_1 =15.53 μH, M_2 =22.08 μH).

and its ON-resistor is 23 mΩ. The diode is STPS30H100CT, and its forward voltage drop is 0.64 V. In the simulation, the ideal compensation network parameters are applied, and the ON-resistance and forward voltage drop of the switching components (i.e., MOSFETs and diodes) is ignored.

B. MIE in Different Rx Placements

As shown in Fig. 3(b), *Rx* can be moved on to the guide rail, and thus different mutual inductances can be created. Fig. 4(a) depicts the relative distance when *Rx* is moved horizontally. The original point ($x_r = 0$ mm) refers that *Rx* is on the central point between *Tx*1 and *Tx*2. M_1 denotes the mutual inductance between *Tx*1 and *Rx*, and M_2 denotes that between *Tx*2 and *Rx*.

Fig. 4(b) and (c) shows two cases such that the horizontal distances of *Rx* are 15 and 10 mm, where the actual mutual inductances are $M_1 = 12.98$ μH and $M_2 = 22.63$ μH, and $M_1 =$ 15.53 μH and $M_2 =$ 22.08 μH, respectively. The estimated mutual inductances in experiments are demonstrated in Fig. 4, and these results are determined by DSP. The relative error of the MIE (i.e., e) is defined as follows:

$$e = \frac{|M_{\text{ac}} - M_{\text{es}}|}{M_{\text{ac}}} \times 100\% \tag{13}$$

where M_{ac} and M_{es} are the actual and estimated mutual inductances, respectively.

The overall experiment and simulation results of the estimated mutual inductance are collected and demonstrated in Fig. 5. The dashed red lines are the actual mutual inductance, and

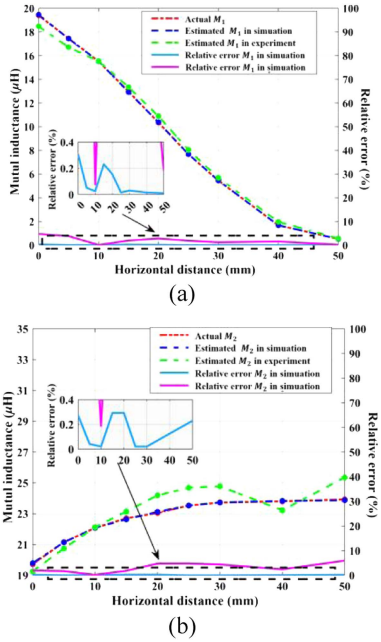

Fig. 5. Experiment and simulation results of estimated mutual inductance and relative error in different horizontal movement distances: (a) M_1 and (b) M_2.

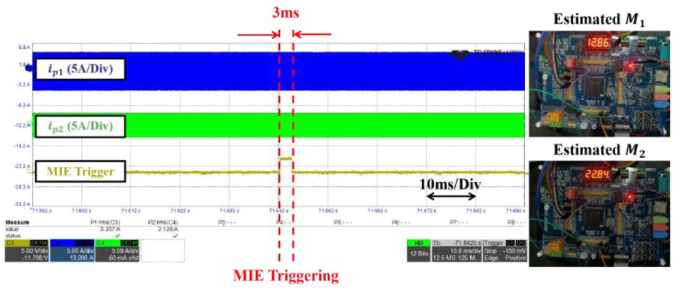

Fig. 6. Dynamic process of the proposed MIE triggered in one cycle under case 1 (x_r = 15 mm, $M_1 = 12.98$ μH, $M_2 = 22.63$ μH).

blue and green lines are the estimated value in simulations and experiments. The solid red lines stand for the relative error. The results shows that the proposed MIE can have lower than 0.3% estimation error in simulation. The maximum relative error in experiment is 6.53%. Under Case 1, the dynamic process of the proposed MIE triggered in one cycle is shown in Fig. 6. It can be observed that the proposed MIE can be processed in 3 ms under dynamic condition.

C. Comparison Study of Related Existing Research Works

In order to further verify the contributions of this work, it is necessary to carry out a comparison study with existing related research works, which have been listed in Table II. It can be seen that the proposed MIE method is without the help of any communication and auxiliary position sensor. Compared with other noncommunication MIE schemes in [8] and [9], the proposed method is much more feasible in multi-*Tx*s DWPT system due to the solution of multiple equations is avoided. Although complex calculation in [10] and [12] is also eliminated, they contain frequency sweeping process in MIE, which means

TABLE II
COMPARISON BETWEEN EXISTING RELATED RESEARCH WORKS

Ref	Configuration	Condition	Communication	Relative error (simulation)	Relative error (experiment)
[5]	One *Tx*-1 Rx	Dynamic	Yes	-	<8%
[6]	One *Tx*-1 Rx	Dynamic	Yes	-	<8%
[7]	Multi-*Tx*s - 1 *Rx*	Dynamic	Yes with speed sensor	-	-
[8]	One *Tx*-1 Rx	Dynamic	No	-	<8%
[9]	One *Tx*-1 Rx	Dynamic	No	<0.1%	<15%
[10]	One *Tx*-1 Rx	Static	No	-	<1.75%
[12]	One *Tx*-1 Rx	Static	No	-	<2%
This work	Multi-*Tx*s - 1 *Rx*	Dynamic	No	<0.1%	<7%

these methods are not suitable for DWPT systems. Based on the aforementioned experimental setup, the proposed MIE can be finished within 3 ms in dynamic conditions. The maximum relative error of the proposed work is <0.1% in simulation and 6.51% in experiment, and it is proven to be comparable with other related researches.

V. CONCLUSION

A new MIE method for SS-compensated multi-*Tx*s DWPT systems is proposed in this letter. The proposed method does not introduce any dual-side communication module. By monitoring only the primary ac winding currents and voltages, the mutual inductance ratio is first determined, and then, the exact mutual inductance is estimated. Because the solution of multivariable multiple equations is not required, the proposed MIE method has low calculation effort, and it has comparable estimation accuracy in resonant frequency. Hence, the proposed method is feasible for DWPT systems with multi-*Tx*s configuration.

REFERENCES

[1] Z. Zhang, H. Pang, A. Georgiadis, and C. Cecati, "Wireless power transfer—An overview," *IEEE Trans. Ind. Electron.*, vol. 66, no. 2, pp. 1044–1058, Feb. 2019.

[2] H. T. Nguyen et al., "Review map of comparative designs for wireless high-power transfer systems in EV applications: Maximum efficiency, ZPA, and CC/CV modes at fixed resonance frequency independent from coupling coefficient," *IEEE Trans. Power Electron.*, vol. 37, no. 4, pp. 4857–4876, Apr. 2022.

[3] Y. Gu, J. Wang, Z. Liang, and Z. Zhang, "Mutual-inductance-dynamic-predicted constant current control of LCC-P compensation network for drone wireless in-flight charging," *IEEE Trans. Ind. Electron.*, vol. 69, no. 12, pp. 12710–12719, Dec. 2022.

[4] Z. Liu, L. Wang, Y. Guo, and S. Li, "Primary-side linear control for constant current/voltage charging of the wireless power transfer system based on the LCC-N compensation topology," *IEEE Trans. Ind. Electron.*, vol. 69, no. 9, pp. 8895–8904, Sep. 2022.

[5] X. Dai, X. Li, Y. Li, and A. P. Hu, "Maximum efficiency tracking for wireless power transfer systems with dynamic coupling coefficient estimation," *IEEE Trans. Power Electron.*, vol. 33, no. 6, pp. 5005–5015, Jun. 2018.

[6] Y. Liu and H. Feng, "Maximum efficiency tracking control method for WPT system based on dynamic coupling coefficient identification and impedance matching network," *IEEE J. Emerg. Sel. Topics Power Electron.*, vol. 8, no. 4, pp. 3633–3643, Dec. 2020, doi: 10.1109/JESTPE.2019.2935219.

[7] D.-H. Kim, S. Kim, S.-W. Kim, J. Moon, I. Cho, and D. Ahn, "Coupling extraction and maximum efficiency tracking for multiple concurrent transmitters in dynamic wireless charging," *IEEE Trans. Power Electron.*, vol. 35, no. 8, pp. 7853–7862, Aug. 2020.

[8] S. Li, L. Wang, Y. Guo, and Z. Liu, "Flexible energy-transfer control of dynamic wireless power transfer system based on estimation of load and mutual inductance," *IEEE Trans. Ind. Appl.*, vol. 58, no. 1, pp. 1157–1167, Jan./Feb. 2022.

[9] V. Jiwariyavej, T. Imura, and Y. Hori, "Coupling coefficients estimation of wireless power transfer system via magnetic resonance coupling using information from either side of the system," *IEEE J. Emerg. Sel. Topics Power Electron.*, vol. 3, no. 1, pp. 191–200, Mar. 2015.

[10] Y. Yang, S. C. Tan, and S. Y. R. Hui, "Fast hardware approach to determining mutual coupling of series-series-compensated wireless power transfer systems with active rectifiers," *IEEE Trans. Power Electron.*, vol. 35, no. 10, pp. 11026–11038, Oct. 2020.

[11] S. A. Khan and D. Ahn, "Coupling estimation and maximum efficiency tracking in multi-transmitters WPT for fast moving receiver," *IEEE Access*, vol. 12, pp. 9952–9962, 2024, doi: 10.1109/ACCESS.2024.3352636.

[12] J. Zeng, Y. Yang, K. Li, S. Chen, and S. Y. R. Hui, "An ultrafast estimation method for coupling coefficient and receiver resonant frequency in universal wireless power transfer systems," *IEEE Trans. Power Electron.*, vol. 39, no. 4, pp. 4870–4883, Apr. 2024.

[13] J. Liu, F. Xu, C. Sun, and K. H. Loo, "A soft-switched power-factor-corrected single-phase bidirectional AC-DC wireless power transfer converter with an integrated power stage," *IEEE Trans. Power Electron.*, vol. 37, no. 8, pp. 10029–10044, Aug. 2022, doi: 10.1109/TPEL.2022.3156577.

[14] J. Liu, F. Xu, C. Sun, and K. H. Loo, "A compact single-phase AC-DC wireless power transfer converter with active power factor correction," *IEEE Trans. Ind. Electron.*, vol. 70, no. 4, pp. 3685–3696, Apr. 2023, doi: 10.1109/TIE.2022.3176297.

[15] A. Garcia-Bediaga, A. Avila, I. Alzuguren, A. Sanchez, and A. Rujas, "Power factor corrector control strategies of a bidirectional wireless battery charger with an unfolding active rectifier," *IEEE J. Emerg. Sel. Topics Power Electron.*, vol. 11, no. 1, pp. 396–406, Feb. 2023, doi: 10.1109/JESTPE.2022.3164720.